The Sensitivity of the Atlantic Meridional Overturning Circulation to Freshwater Forcing at Eddy-Permitting Resolutions

J. PAUL SPENCE, MICHAEL EBY, AND ANDREW J. WEAVER

School of Earth and Ocean Sciences, University of Victoria, Victoria, British Columbia, Canada

(Manuscript received 18 June 2007, in final form 2 October 2007)

ABSTRACT

The effect of increasing horizontal resolution is examined to assess the response of the Atlantic meridional overturning circulation (AMOC) to freshwater perturbations. Versions of a global climate model with horizontal resolutions ranging from 1.8° (latitude) × 3.6° (longitude) to 0.2° × 0.4° are used to determine if the AMOC response to freshwater forcing is robust to increasing resolution. In the preindustrial equilibrium climate, the representation of western boundary currents and meridional heat transport are improved with resolution. Freshwater forcings similar to the final drainage of proglacial Lakes Agassiz and Ojibway are applied evenly over the Labrador Sea and exclusively along the western boundary. The duration and maximum amplitude of model responses to freshwater forcing showed little sensitivity to increasing resolution. An evaluation with tracers of the forcing impact on different regions of North Atlantic Deep Water formation revealed the possibility that increases in Labrador Sea deep convection at higher resolution mitigate the effect of stronger boundary currents and enhanced mixing. With increasing resolution, there is less cooling in the subpolar west Atlantic, more cooling in the subpolar east Atlantic, and greater variability in the deep ocean response to the boundary forcing. While differences exist, the coarse-resolution model response remains robust at finer horizontal resolutions.

1. Introduction

Variation in the poleward transport of heat by the Atlantic meridional overturning circulation (AMOC) is commonly evoked as a mechanism to explain large-scale climate events found in paleorecords (Bond et al. 1993; Rahmstorf 2002). A wide range of modeling studies have demonstrated a weakened AMOC in response to surface freshwater forcing at North Atlantic Deep Water (NADW) formation sites (e.g., Stommel 1961; Weaver and Hughes 1992; Stouffer et al. 2006); specifically, an increased freshwater flux creates more stably stratified surface water, which reduces deep water formation and its concomitant meridional heat transport, producing a cooling of Northern Hemisphere climate. Because the deep ocean requires centuries to millennia to reach a thermodynamic equilibrium (Broecker 1991), computational constraints have historically limited the horizontal resolution of models used in previous studies to greater than 1° (latitude) × 1° (longitude). A number of important oceanic processes are not adequately represented at coarse (>1°) resolution. For example, the widths of boundary currents are overestimated, while their speeds are underestimated, and the influence of mesoscale eddies are fairly crudely parameterized. The Intergovernmental Panel on Climate Change (IPCC) Third Assessment Report (TAR) warned that model results reliant on meridional heat transports with >1° resolution ocean components should be treated cautiously (McAvaney et al. 2001). The IPCC TAR reported that a lack of experiments exploring the impacts of resolution restricts the ability to draw firm conclusions. We address this need by investigating AMOC variability in a series of global models with horizontal resolutions increasing into the ocean eddy-permitting range.

Of the few studies that have systematically examined the effects of increasing model resolution, none evaluated differences in the response to deep water formation perturbations. Earlier research focused on ocean volume and heat transports at (or near) equilibrium with model domains limited to the Atlantic basin (e.g., Bryan 1991; Beckmann et al. 1994; Böning et al. 1996;

Corresponding author address: J. Paul Spence, School of Earth and Ocean Sciences, University of Victoria, P.O. Box 3055, Victoria, BC V8W 3P6, Canada.
E-mail: pspence@ocean.seos.uvic.ca

DOI: 10.1175/2007JCLI2103.1

Fanning and Weaver 1997, 1998; Smith et al. 2000; Oschlies 2002). Duffy et al. (2002) evaluated the unperturbed state in a set of global Earth System Models of Intermediate Complexity (EMICs), but the finest-resolution model was $1° \times 1°$. In this paper we evaluate model states before and after applying freshwater forcing similar to the 8.2-kyr event.

The 8.2-kyr event refers to the widespread cooling found in paleoclimate records in Greenland, Europe, North America, and the tropical Atlantic roughly 8200 calendar years ago (Alley and Agustsdottir 2005; Morrill and Jacobsen 2005). The forcing for this event is thought to be the catastrophic final drainage of proglacial Lakes Agassiz and Ojibway (hereafter Lake Agassiz) into Hudson Bay and the Labrador Sea (Barber et al. 1999). Paleoevidence suggests that roughly 1.65×10^{14} m^3 of freshwater drained in less than a year (equivalent to twice the volume of the present-day Caspian Sea), creating one of the largest abrupt climate events of the Holocene (Leverington et al. 2002; Clarke et al. 2003).

In this study, we advance the equilibration of high-resolution models by initiating them from an interpolated equilibrium state of a lower-resolution EMIC. Models with horizontal resolutions of $0.6°$ (latitude) $\times$ $1.2°$ (longitude), $0.3° \times 0.6°$, and $0.2° \times 0.4°$ are further integrated from the 3000-yr state of a $1.8° \times 3.6°$ model. The two highest-resolution models have grid spacings that are finer than typical ocean eddy wavelengths (100–200 km) (Stammer 1997), but coarser than the Rossby radius of deformation at high latitudes (Smith et al. 2000; Oschlies 2002), which qualifies them as eddy permitting. All models are integrated under orbital, atmospheric (CO_2 = 280 ppm), and land surface conditions corresponding to the year 1850, rather than 8.2-kyr conditions (CO_2 = 260 ppm), so that they may be used in future studies of anthropogenic warming. The exclusion of many forcings specific to the 8.2-kyr event limits a detailed comparison to proxy evidence.

Two freshwater perturbation scenarios are investigated at each model resolution. In the first, we follow previous modeling studies (e.g., Renssen et al. 2001; Bauer et al. 2004; Wang and Mysak 2005) by distributing the freshwater uniformly over the entire Labrador Sea. However, most of the transport of the North Atlantic subpolar gyre occurs in coastal boundary currents, and it is likely that much of the freshwater discharged by the 8.2-kyr event would have been confined initially to the continental margin (Wunsch 2006). The ability of boundary currents to influence the AMOC response is investigated in the second scenario, wherein the freshwater is applied along the coastline of northeast North America. Our working hypothesis is that stronger boundary currents and enhanced mixing in higher-resolution models may act to mitigate the AMOC response to freshwater forcing. The purpose of this study is to determine if the coarse-resolution AMOC response remains robust at finer horizontal resolutions.

The outline of the remainder of this paper is as follows: Section 2 describes the climate model and the experimental design. In section 3 we evaluate model states prior to forcing, and section 4 examines the response to the 8.2-kyr event freshwater forcing scenarios. Conclusions are presented in section 5.

2. Model description and experimental design

a. The University of Victoria Earth System Climate Model

This study uses version 2.7 of the intermediate complexity University of Victoria Earth System Climate Model (UVic ESCM). The UVic ESCM couples a 3D ocean general circulation model, a 2D atmospheric model, a thermodynamic–dynamic sea ice model, and a simple land surface model, described in detail in Weaver et al. (2001). The UVic ESCM has a global domain, and model components share the same horizontal grid resolution.

The ocean component is version 2.2 of the Geophysical Fluid Dynamics Laboratory Modular Ocean Model (Pacanowski 1995). It has 19 vertical levels that increase parabolically in thickness from 50 m at the surface to 518 m at the deepest level. The vertical diffusivity ranges from 3.0×10^{-5} m^2 s^{-1} near the surface to 1.3×10^{-4} m^2 s^{-1} at depth, according to the scheme of Bryan and Lewis (1979). Mixing associated with mesoscale eddies is parameterized according to Gent and McWilliams (1990). Isopycnal and horizontal viscosity coefficients were chosen based on the horizontal resolution of each model, with details provided in the following subsection. The barotropic momentum equations are solved by the implicit free-surface formulation of Dukowicz and Smith (1994). Surface freshwater fluxes are converted to fluxes of salt with a constant salt-to-freshwater mass ratio of 3.49×10^{-2}.

The sea ice model incorporates energy-conserving ice–snow thermodynamics with a two-category thickness distribution (Hibler 1979) and an elastic–viscous–plastic rheology (Hunke and Dukowicz 1997). The model predicts ice thickness, areal fraction, and surface temperature.

The UVic ESCM employs a vertically integrated energy–moisture balance atmospheric model for computational efficiency. Precipitation occurs when the relative humidity exceeds 90%, and on land it is treated by

TABLE 1. Horizontal resolution parameters and salient features of North Atlantic climate in control runs. The terms A_M, A_{ISO}, and A_{ITH} are the horizontal, isopycnal, and isopycnal thickness diffusion coefficients, respectively. Subtropical and subpolar transport refers to the maximum barotropic transport found within the gyres. The Gulf Stream and Labrador Current speeds are the maximum near-surface speeds located within 2°-wide meridional bands centered along 68° and 55°W, respectively. Total potential energy released by ocean convection was calculated from grid cells with a ventilation depth >300 m over the months of January, February, and March in the last year of the control runs.

Horizontal resolution	1.8° × 3.6°	0.6° × 1.2°	0.3° × 0.6°	0.2° × 0.4°
A_M ($\times 10^8$ cm^2 s^{-1})	20	7	3	1.5
A_{ISO} and A_{ITH} ($\times 10^6$ cm^2 s^{-1})	4	1.5	1	0.75
Integration time (yr)	3000	450	100	50
Subtropical transport (Sv)	44.3	48.9	52.9	49.1
Gulf Stream current speed (cm s^{-1})	23.4	38.7	47.4	52.1
Subpolar transport (Sv)	−25.9	−24.4	−27.9	−27.2
Labrador Current speed (cm s^{-1})	3.5	11.2	13.3	17.4
Total convection energy ($\times 10^{17}$ J)	9.2	9.2	7.8	7.7
Labrador Sea convection energy ($\times 10^{16}$ J)	0.6	10.5	8.4	5.2
(Labrador Sea energy × 100)/total	0.7%	11.4%	10.8%	6.8%

a simple bucket model described in Matthews et al. (2003). The UVic ESCM is forced from start-up by insolation and surface winds. Winds are prescribed from the long-term monthly mean climatology of the National Centers for Environmental Prediction–National Center for Atmospheric Research (NCEP–NCAR) 50-Year Reanalysis (Kistler et al. 2001) and interpolated to match model resolutions.

b. Experimental design

All models are integrated under preindustrial (year 1850) orbital, atmospheric, and land surface conditions. Table 1 lists the values of the primary parameters modified in each model as well as their preforcing integration times. The number of vertical ocean levels is held fixed and the bathymetry is left unchanged with resolution. We simply divide the 1.8° × 3.6° bathymetry into higher-resolution grids. For example, a 0.6° × 1.2° bathymetry is constructed by dividing each cell in the 1.8° × 3.6° bathymetry matrix into a 3 × 3 matrix. This technique allows us to focus on the resolution of ocean boundary currents and boundary layer freshwater flux forcing, while excluding both the attributes and complications arising from flows through regions of complex bathymetry. The horizontal resolution of the land, atmosphere, and sea ice components are also increased in the same manner as the bathymetry. All experiments use the same values for vertical ocean mixing coefficients.

The thermocline time scale required for adjustment to the perturbation induced upon switching resolution should be comparable to that for a first-mode Rossby wave to cross the basin (roughly 30 yr; Fanning and Weaver 1997). The integration times of the two eddy-permitting models exceed the thermocline adjustment time scale, but are not sufficient to remove all of the long-time-scale transients in the deep ocean. Time step interval data do not show a consistent linear trend in potential temperature, but a weak linear salinity trend of roughly 0.0040 psu per century is evident in the three higher-resolution models. By the end of the control equilibrations, the range of global mean ocean potential temperature and salinity among the models is 3.63–3.65 K and 34.79–34.81 psu, respectively.

We simulated the 8.2-kyr event by adding 1.65×10^{14} m^3 of freshwater to the surface of the Labrador Sea. To prevent the converted salt flux from generating negative salinity values, we applied freshwater at a rate of 1.75 Sv (1 Sv $\equiv 10^6$ m^3 s^{-1}) for a period of 3 yr. Two perturbation scenarios were carried out for each control run. In the first scenario (hereafter LAB forcing), the freshwater was distributed uniformly over the entire Labrador Sea (Fig. 1a). In the second scenario (hereafter BC forcing), the freshwater was applied as close as possible to the coastline of northeastern North America (Fig. 1b). For the 1.8° × 3.6° model (Fig. 1b), the boundary forcing region was one grid box wide. For the three higher-resolution models, the boundary forcing region was two grid boxes wide.

3. Evaluation of preforcing climate states

a. North Atlantic barotropic circulation

Because the topography and applied wind stress curl are the same in each model, linear Sverdrup theory predicts equivalent barotropic ocean volume transports. Pronounced differences should occur in both the North Atlantic subpolar gyre and the western boundary of the subtropical gyre, where the local dynamics are

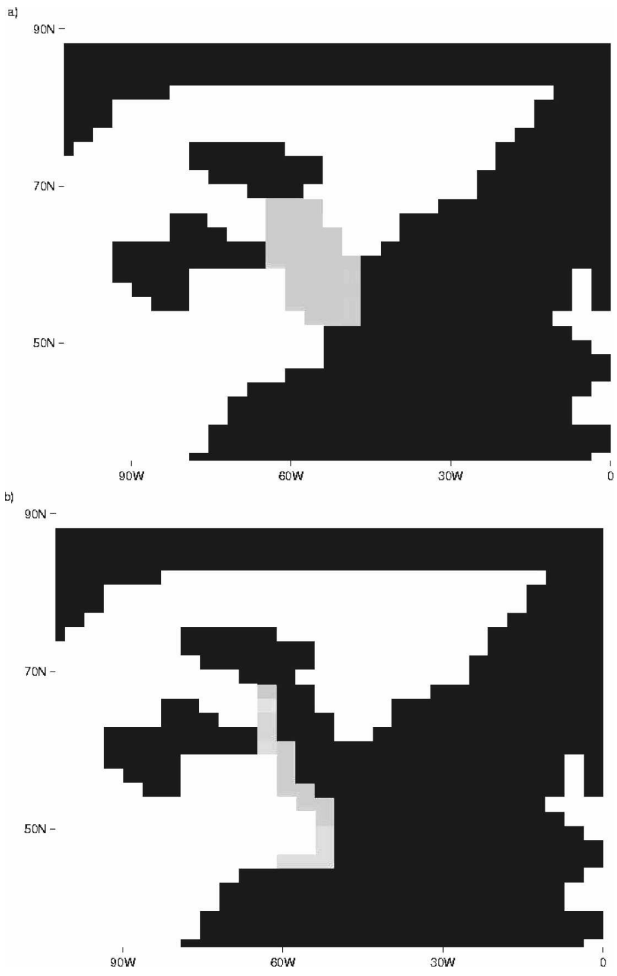

FIG. 1. (a) In the LAB forcing scenario, the freshwater was distributed over the gray region, the size of which is independent of horizontal resolution. (b) In the BC forcing scenario, the freshwater was applied to a coastal strip one grid cell wide in the $1.8° \times 3.6°$ model, and (not shown) to a coastal strip two grid cells wide in the higher-resolution models.

nonlinear and significantly influenced by deep water flows (Bryan et al. 1995).

Figure 2 shows the annual mean North Atlantic barotropic streamfunction for the last year of the control runs at each resolution. In the subtropical gyre, our simulations follow Sverdrup theory as similar transports are produced in the eastern half of the gyre, while differences dominate near the western boundary. The width of the western boundary transport is more realistically represented at higher resolution; it is considerably narrowed and restricted to the edge of the continental shelf. The maximum barotropic transport within the subtropical gyre (Table 1) in all of our simulations compares favorably to other studies, with the three highest-resolution models showing a 9%–16% increase (not monotonically) in transport relative to the coarse model (Beckmann et al. 1994; Smith et al. 2000; Oschlies 2002). However, the modeled transport remains smaller than the observed estimate of 88 Sv along 68°W made by Johns et al. (1995). The simulated maximum near-surface current speed along 68°W increases from 23.4 to 52.1 cm s^{-1} in going from $1.8° \times 3.6°$ to $0.2° \times 0.4°$, but remains less than the observed value of 70 cm s^{-1} (Johns et al. 1995). The surface velocity field (not shown) confirms that the separation of the Gulf Stream into the Azores and North Atlantic Current (NAC) is significantly improved at higher resolution and corresponds with a greater poleward penetration of the NAC.

The dynamics of the North Atlantic subpolar gyre present an exceptional modeling challenge because of the complex interaction between wind forcing, buoyancy contrasts, and overflows from neighboring seas. Detailed modeling studies have shown encouraging but limited results in simulating observed currents and water mass characteristics in this region (Willebrand et al. 2001; Treguier et al. 2005). The overall structure and magnitude of the subpolar gyre transport remains fairly consistent with increasing resolution in our study (Fig. 2). However, the maximum transports of the subpolar gyre (Table 1) are low in comparison to regional models, one of which [the French Atlantic (ATL) model] showed an increase in the maximum transport from 25 Sv to 40 Sv upon switching from coarse to high resolution (Treguier et al. 2005). The relatively low subpolar gyre transports in our higher-resolution model likely results from us maintaining the same coarse topography as we increased horizontal resolutions. An increase in the transport off the coast of Labrador in our models results from the penetration of the subpolar gyre further into the Labrador Sea at higher resolution. The maximum near-surface speed of the Labrador Current at 55°W (Table 1) increases from 3.5 to 17.4 cm s^{-1} between our coarsest- and highest-resolution models, but remains low in comparison to the observed values of roughly 30 cm s^{-1} (Flatau et al. 2003).

b. Atlantic meridional overturning circulation

AMOC transport in the model is depicted by the annual mean streamfunction of the zonally integrated volume transport. Figure 3a shows that 21 Sv of NADW formation occurs in the $1.8° \times 3.6°$ model, although, with a maximum poleward extent of 60°N, it has a tendency to form too far south. This deficiency results from the model's inability to transport surface waters effectively across the Iceland–Faroes ridge, which leads to the AMOC not penetrating far enough into the Greenland–Iceland–Norwegian (GIN) Seas (Weaver et al. 2001). Observational estimates of the

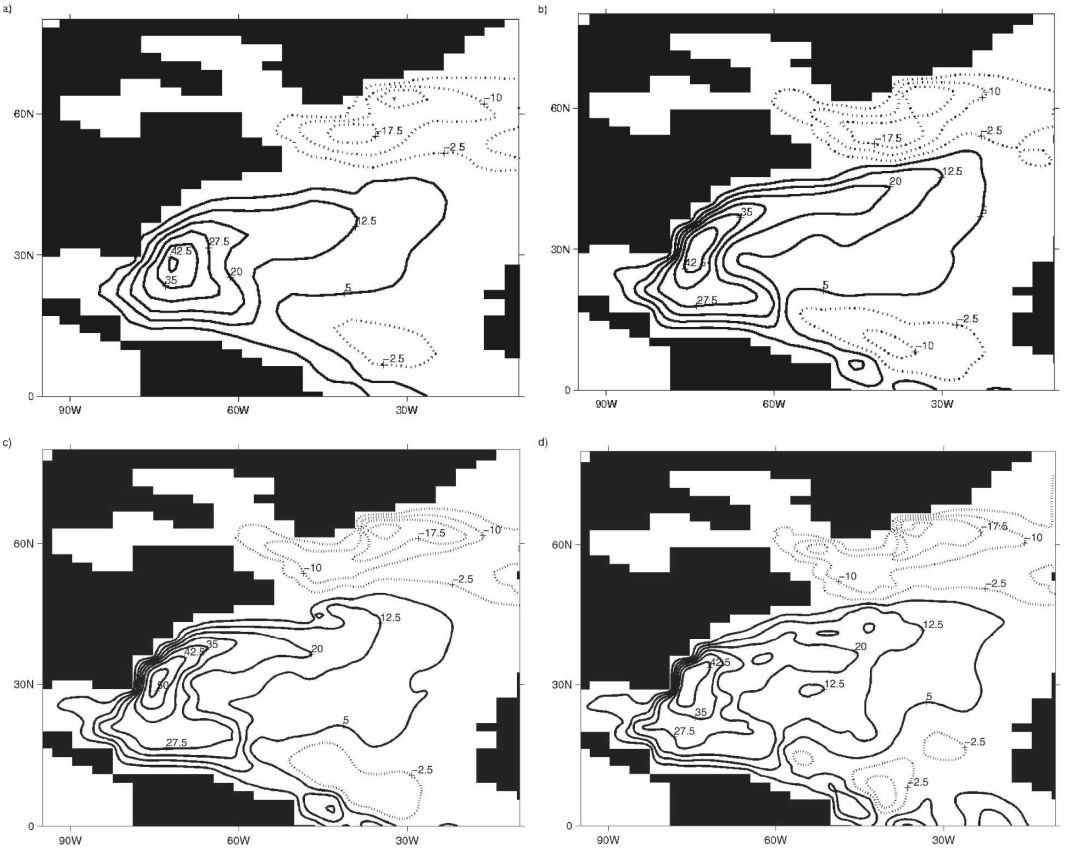

FIG. 2. Annual mean barotropic streamfunction (Sv) for the North Atlantic in the control runs. Horizontal resolutions are (a) 1.8° × 3.6°, (b) 0.6° × 1.2°, (c) 0.3° × 0.6°, and (d) 0.2° × 0.4°. Dotted lines are negative.

present-day NADW volume transport range from 13 to 23 Sv (Ganachaud and Wunsch 2000; Smethie and Fine 2001; Lumpkin and Speer 2003; Talley et al. 2003). Approximately 1.5 Sv of Antarctic Bottom Water (AABW) is found extending to 25°N and fills the North Atlantic below 3000 m.

We find little difference in the overall structure and magnitude of AMOC transport among the three higher-resolution models. In comparison to the 1.8° × 3.6° model, there is an increase of 1–2 Sv in NADW formation and a significantly improved poleward penetration to 75°N. AABW transport increases slightly in these runs and extends slightly farther north. The most significant change in AABW transport is found in the 0.6° × 1.2° model, with 2.5 Sv of transport at 25°N and 0.5 Sv extending to 40°N.

c. *Meridional heat transport*

Ganachaud and Wunsch (2003) used observational data to estimate the present-day global ocean poleward heat transport to be 1.8 PW (1 PW ≡ 10^{15} watts) at 24°N, with ~70% occurring in the Atlantic. Studies have shown that the large-scale ocean heat transport is dominated by the mean circulation (Wunsch 1999; Talley 2003). However, locally the heat transport by small-scale and time-varying circulations can be of first-order importance, influencing the large-scale heat transport directly via advection and indirectly by modifying the mean flow and surface heat flux budgets (Stammer 1997). Regional modeling studies have demonstrated a dependence of ocean heat transport on resolution, with coarse-resolution models generating poleward transports that are significantly less than those observed (Fanning and Weaver 1997; Bryan and Smith 1998).

We find that the global ocean meridional heat transport increases with increasing resolution while maintaining the same transport profile (Fig. 4). Each model exhibits poleward transport at all latitudes and a strong asymmetry across the equator. At 24°N there is an almost 30% increase in total oceanic heat transport (1.2 to 1.7 PW) by changing from 1.8° × 3.6° to 0.2° × 0.4° resolution. The increase in transport is largely associated with the better resolution of the western boundary currents in the baroclinic gyre circulations, which are

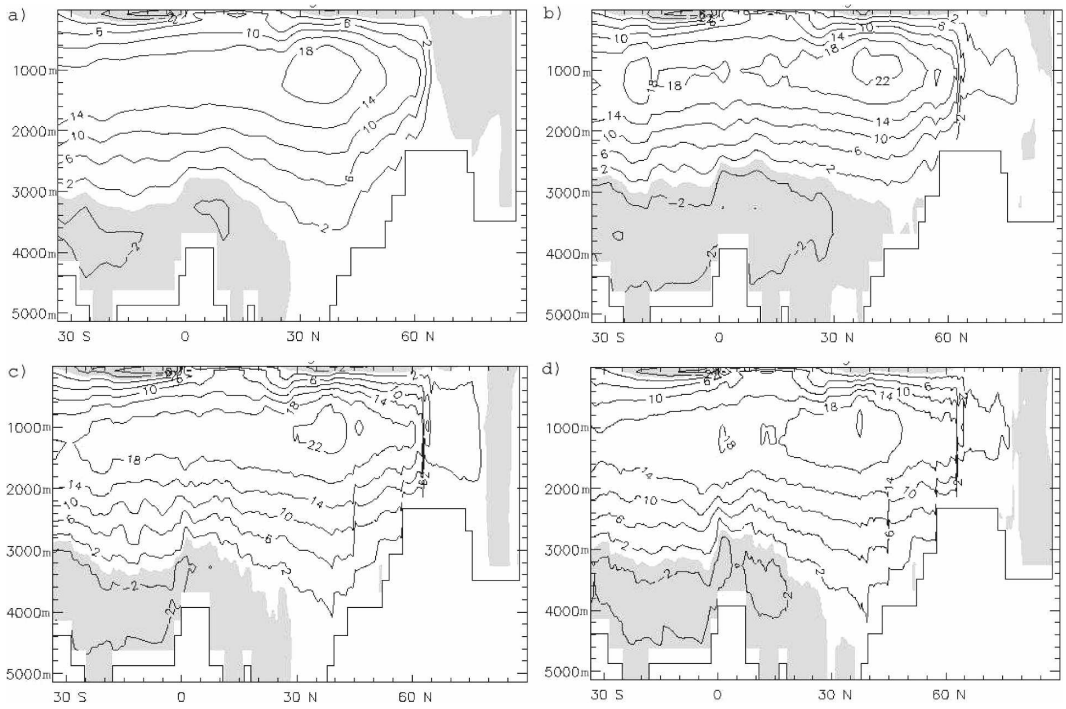

FIG. 3. Annual mean meridional overturning streamfunction (Sv) for the North Atlantic in the control runs. Horizontal resolutions are (a) 1.8° × 3.6°, (b) 0.6° × 1.2°, (c) 0.3° × 0.6°, and (d) 0.2° × 0.4°. Shaded regions are negative.

significant components of the transport in the mid-to-high latitudes. Our results demonstrate that increases in horizontal resolution produce meridional heat transports that are closer to the observed values, consistent with the findings of Fanning and Weaver (1997) and Bryan and Smith (1998).

d. NADW formation

Open ocean deep convective mixing, triggered by extreme surface cooling events during the North Atlantic winter, is an important process in the formation of NADW (Weaver and Hughes 1992; Dickson and Brown 1994; Marshall and Schott 1999). The methods used to parameterize this process in models are widely debated (Canuto et al. 2004; Treguier et al. 2005). The UVic ESCM employs an explicit full convection scheme, which includes diagnostics to save the ventilation depth and potential energy released by convection at each grid point (Pacanowski 1995).

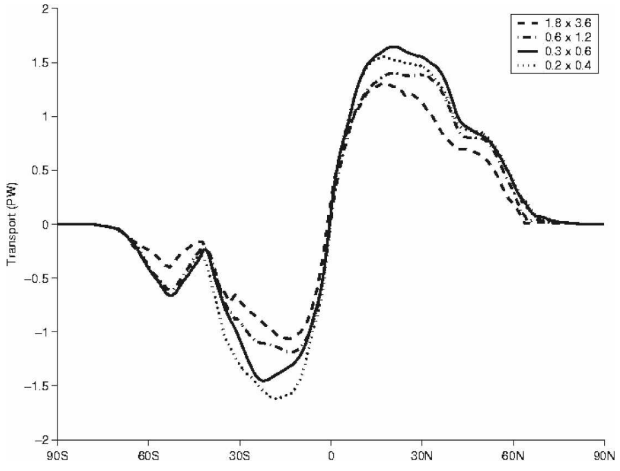

FIG. 4. The total meridional heat transport for the global ocean for each model resolution.

Figure 5 shows the depth of convective activity in the North Atlantic averaged over the winter months (January–March) in the last year of the control runs. None of the models exhibit a significant amount of interannual variability in the magnitude or location of convection. In all four models, deep (>300 m) convective activity occurs predominately in the GIN Seas, albeit too far south. While the poleward penetration of the NAC is improved at higher resolution, it apparently still does not transport surface waters across the Iceland–Faroes Ridge effectively enough to provide suitable conditions for deep convection. The most striking difference between models is the occurrence of convective activity in the Labrador Sea, and to a lesser extent the Irminger Sea, in all but the coarsest-resolution model. To quantify this difference, we summed the potential energy released by deep winter convection over the entire subpolar gyre region and exclusively over the Labrador

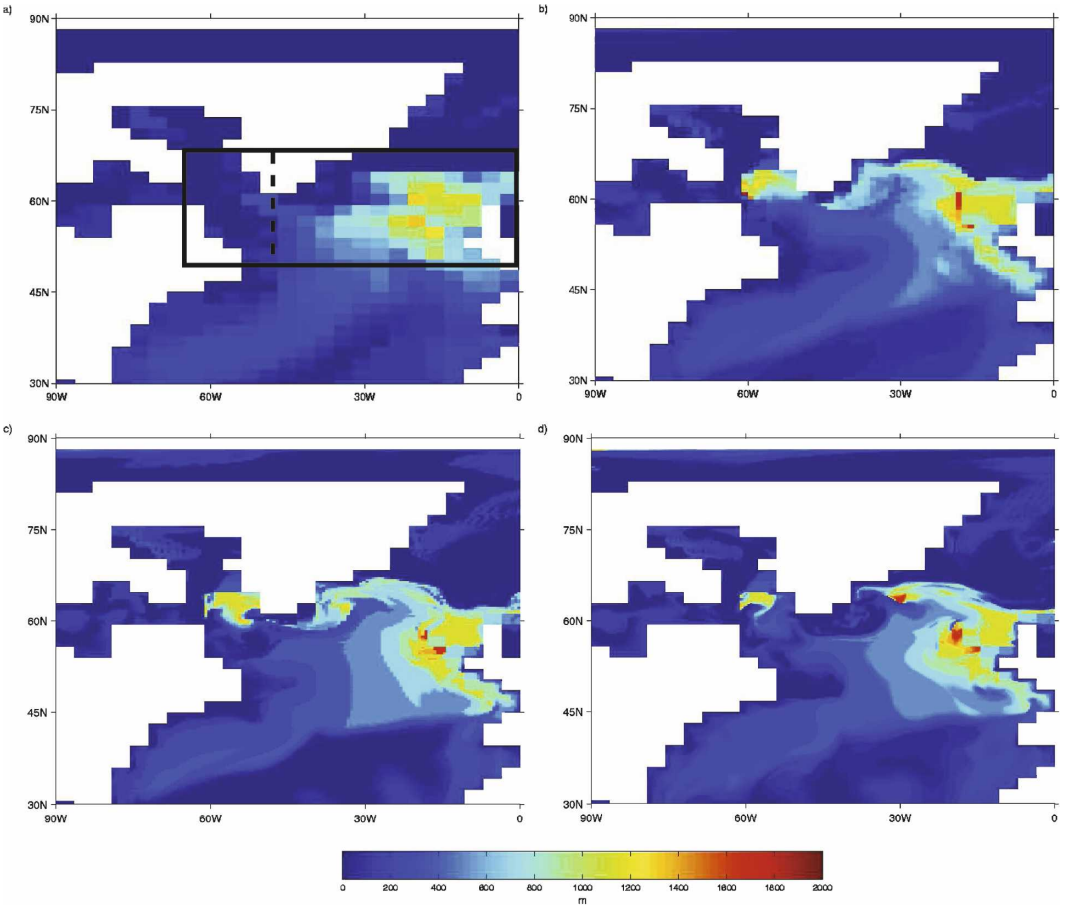

FIG. 5. Ventilation depth of convective activity in the North Atlantic averaged over January, February, and March in the last year of the preforcing runs. Horizontal resolutions are (a) 1.8° × 3.6°, (b) 0.6° × 1.2°, (c) 0.3° × 0.6°, and (d) 0.2° × 0.4°. The vertical dashed line extending southward from the tip of Greenland in (a) distinguishes the Labrador Sea region from the total area (indicated by the large black box) where the potential energies for Table 1 were calculated.

Sea (Fig. 5a defines these regions). The results, shown in Table 1, demonstrate a significant contribution from the Labrador Sea to the total convective energy in all but the coarsest model. The depth of the Labrador Sea convection compares well with the observations of Lavender et al. (2002). There is also a 15% decrease in the total Atlantic convective energy in the two eddy-permitting models.

To evaluate how differences in the location of convective activity affect the formation of NADW, we applied three inert tracers to the ocean surface in the 1.8° × 3.6°, 0.6° × 1.2°, and 0.3° × 0.6° control runs. Computational constraints prevented us from applying tracers in the 0.2° × 0.4° model. Tracer 1 was applied to the region of convective activity in the GIN Seas, tracer 2 was applied to the Labrador Sea, and tracer 3 was applied everywhere else in the global ocean (hereafter the LAB, GIN, and GLOBAL tracers, respectively). A constant flux (0.1 Sv) of each tracer was applied to the ocean surface in each control run and integrated in parallel with the freshwater forcing runs (in which tracers were also applied) for an additional 50 yr. We are able to estimate the percentage and location of NADW that originated at the surface of the Labrador and GIN Seas (ignoring advection of the tracers at the surface) by zonally integrating the three tracers across the Atlantic basin and then calculating the percentage of each relative to the total amount of tracers in a grid cell. Figure 6 shows the distribution of tracers in the 1.8° × 3.6° and 0.3° × 0.6° models after 50 yr. The 0.3° × 0.6° model fairly represents the tracer distributions in the 0.6° × 1.2° model, which also exhibits extensive convection in the Labrador Sea. It should be noted that very small amounts of tracers are found below 4000 m, resulting in tracer percentages that are not indicative of significant amounts of NADW.

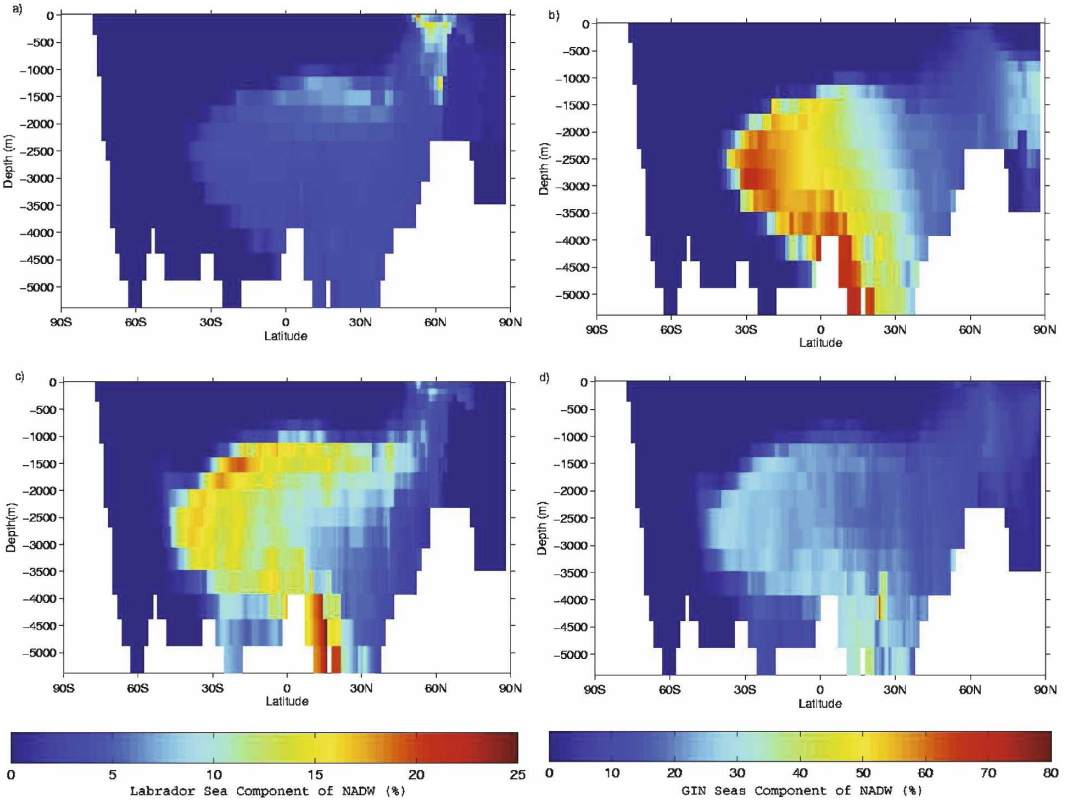

FIG. 6. The percentage of NADW identified by tracers to have originated in the Labrador Sea for the (a) 1.8° × 3.6° and (c) 0.3° × 0.6° models. (b), (d) Same as (a), (c) but for the percentage of NADW that originated in the GIN Seas. Different color bar scales are used for the GIN and LAB tracer percentages.

The models clearly simulate the sinking and spreading of NADW below the permanent thermocline to a depth of 3500 m at 30°S, where after 50 yr the tracers tend to accumulate and override AABW. Figure 6 reveals additional significant differences between the models in the surface source regions of NADW. In the 1.8° × 3.6° model, ~5% of NADW originated in the Labrador Sea (Fig. 6a), while GIN tracers comprise ~55% (Fig. 6b). In the 0.3° × 0.6° model, ~15% of NADW originated in the Labrador Sea (Fig. 6c), while ~40% of the tracers originated at the surface of the GIN Seas (Fig. 6d). The GLOBAL tracer makes up the residual percentages, which amounts to roughly ~40% and ~45% for the 1.8° × 3.6° and 0.3° × 0.6° models, respectively. Figure 6 shows that while similar amounts of NADW are formed, a greater percentage of it originated at the surface of the Labrador Sea in the higher-resolution model.

e. Sea ice distribution

At its standard resolution (1.8° × 3.6°), the UVic ESCM produces sea ice climatology that favorably compares to observations (Weaver et al. 2001). However, the fact that NADW forms too far south leads to a sea ice cover that extends too far south in the North Atlantic, especially in the GIN Seas (Fig. 7a). As horizontal resolution is increased, there is a significant reduction in North Atlantic sea ice extent, particularly in the region of the Norwegian Current, and to a lesser extent in the Labrador Sea and Hudson Bay (Figs. 7b–d). The annual average Northern Hemisphere sea ice volume in the 1.8° × 3.6° model is 9.3×10^{12} m^3. It is reduced by 6.5%, 8.6%, and 9.2% as resolution is increased to 0.6° × 1.2°, 0.3° × 0.6°, and 0.2° × 0.4°, respectively. The monotonic pattern of North Atlantic sea ice reduction in response to increased horizontal resolution is consistent with our findings of increased meridional heat transport and greater poleward penetration of AMOC surface waters at higher resolutions.

4. Response to the 8.2-kyr event freshwater forcing

a. AMOC response

The principal means of detecting changes in NADW formation is to examine changes in the maximum value of AMOC transport between the latitudinal bounds of

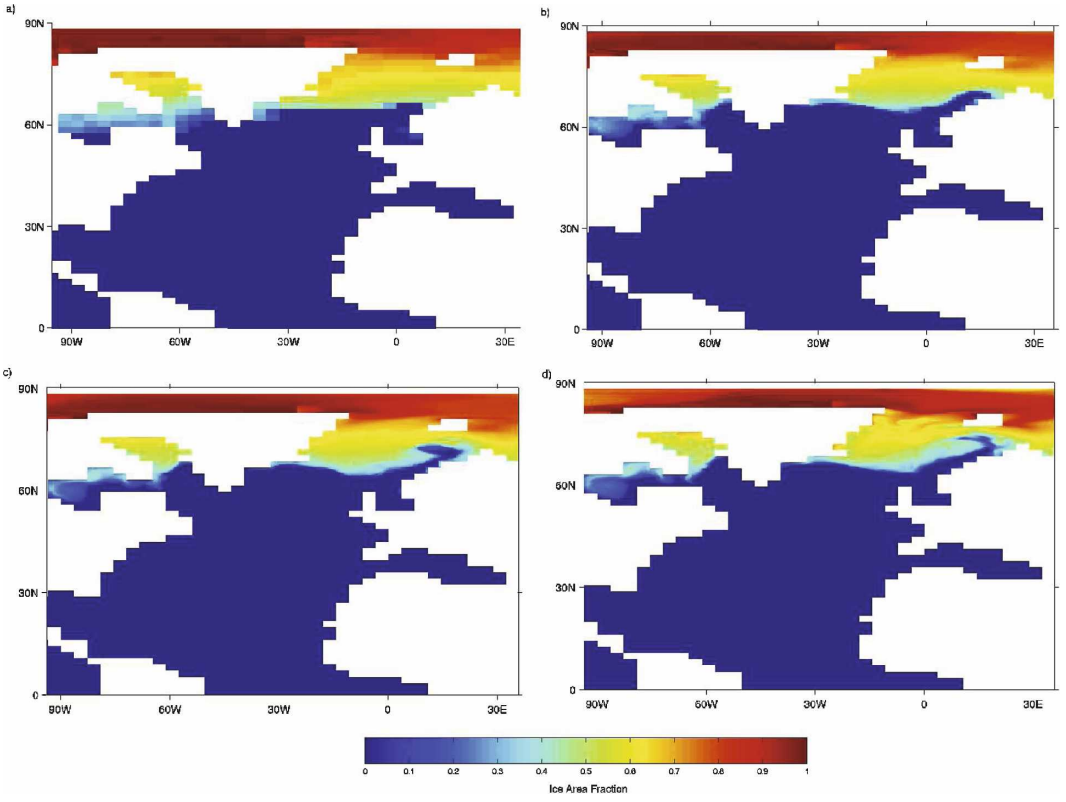

FIG. 7. The annually averaged fraction of each ocean grid cell covered by ice. Horizontal resolutions are (a) 1.8° × 3.6°, (b) 0.6° × 1.2°, (c) 0.3° × 0.6°, and (d) 0.2° × 0.4°.

26° and 70°N, and depths of 170 and 4000 m (hereafter, the AMOC strength). The 1.8° × 3.6° model produces a preindustrial equilibrium AMOC strength of 21 Sv with little internal variability (Fig. 8). At 0.6° × 1.2° and 0.3° × 0.6°, the AMOC equilibrates at ~23 Sv, while at 0.2° × 0.4° the AMOC strength tends to decline slightly from ~23 Sv to ~21.5 Sv prior to forcing (Fig. 8). The internal variability in NADW formation is significantly increased in the three highest-resolution models.

The overall response of the AMOC to the LAB forcing scenario is consistent among the models (Fig. 8a). All exhibit near immediate reductions in the rate of NADW formation and subsequently recover. The total duration (ranges from 40–60 yr) and maximum amplitude (ranges from 4–7 Sv) of the AMOC response does not have a consistent dependence on model resolution. However, there are subtle differences in the pathway of the response. The initial decline in the 1.8° × 3.6° model is followed by a brief period of reintensification (starting 5 yr after forcing) before smoothly recovering, in accord with the coarse-resolution model results presented by Manabe and Stouffer (1995), Renssen et al. (2002), and Bauer et al. (2004). Over the first 10 yr, the 0.6° × 1.2° model follows a path similar to the 1.8° × 3.6° model, but has a second reintensification phase (20 yr after forcing) that precedes another relatively small decline in AMOC strength before recovery. Neither the 0.3° × 0.6° nor the 0.2° × 0.4° model shows a reintensification phase within the first 10 yr. Instead they exhibit a reintensification similar to the second phase of the 0.6° × 1.2° model.

There are substantial differences in the pathway of the AMOC response to the BC forcing scenario (Fig. 8b). First, all four models exhibit a strong reintensification within the first 5 yr of the response. The three highest-resolution models also show a substantial second reintensification that is followed by a significant third phase of reduced NADW formation before recovery. While the maximum amplitude of decline in AMOC strength and total duration of the response are similar to that found for the LAB forcing, there are higher-amplitude variations in the BC forcing response of all four models.

b. *Surface air temperature response*

The transient response of the annual average Northern Hemisphere surface air temperature (SAT) is rela-

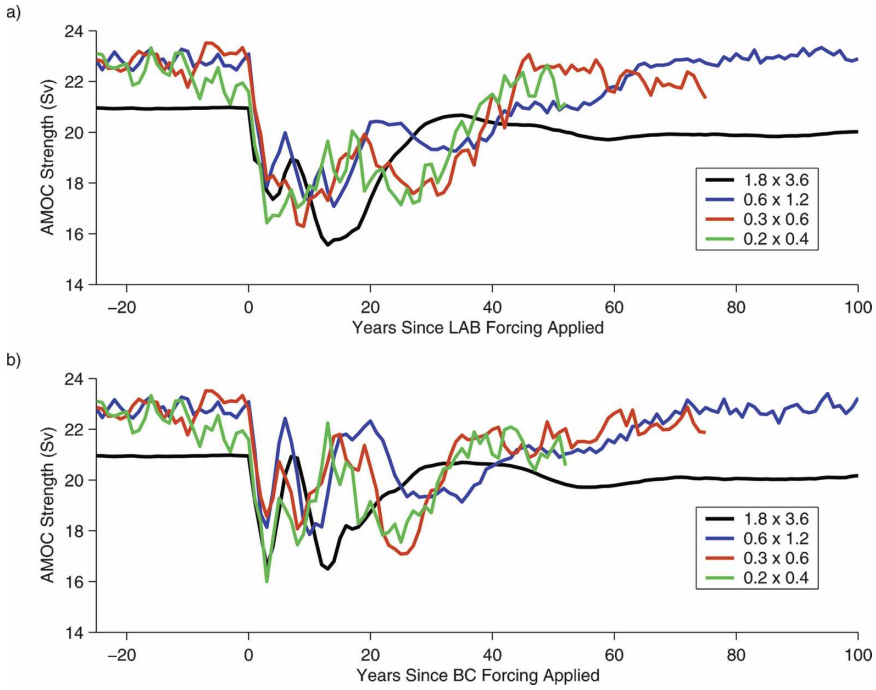

FIG. 8. The AMOC strength of each model over the 25-yr period prior to forcing, and the response to the (a) LAB and (b) BC freshwater forcing scenarios.

tively insensitive to differing model resolutions and forcing regions (Fig. 9). A rapid cooling of roughly 0.4°C within the first 5 yr is found in all models for both the BC and LAB scenarios. The cold period is sustained for at most a few years as it enhances the meridional temperature gradient, which induces a poleward advection of heat in the North Atlantic. After 20 yr the Northern Hemisphere SAT recovers, exceeding the preforcing values by ~0.1°C in all but the highest-resolution model. This warming is followed by another cooling phase resulting from the lagged restoration of deep convection; a response previously described by Manabe and Stouffer (1995) and Renssen et al. (2002). The total duration of the SAT response (50 yr) is consistent among the models, but much shorter than the 200-yr anomaly inferred from paleodata. Previous studies highlighted the importance of long-term changes in the routing of glacial runoff, along with the abrupt drainage of Lake Agassiz, as an important mechanism for extending the duration of the 8.2-kyr event (Bauer et al. 2004; Meissner and Clark 2006).

The spatial pattern of the SAT response to the LAB forcing is also relatively insensitive to increasing model resolution. Global SAT anomalies 5 yr after the initial forcing for the 0.3° × 0.6° model are representative of the other models (Fig. 10a). The SAT decreases by 0.4°–2.4°C over the North Atlantic and Europe, which is within the range of estimates from paleorecords (Bond et al. 1997; Von Grafenstein et al. 1998). A warming signal in the range of 0.2°–0.6°C is found poleward of 30°S, which is consistent with the interhemispheric seesaw nature of heat transport identified in previous modeling studies (Stocker 1998).

All models produce less cooling in the subpolar west Atlantic and more cooling in the subpolar east Atlantic in response to the BC forcing (Fig. 10b). This effect is enhanced with increasing resolution: the maximum

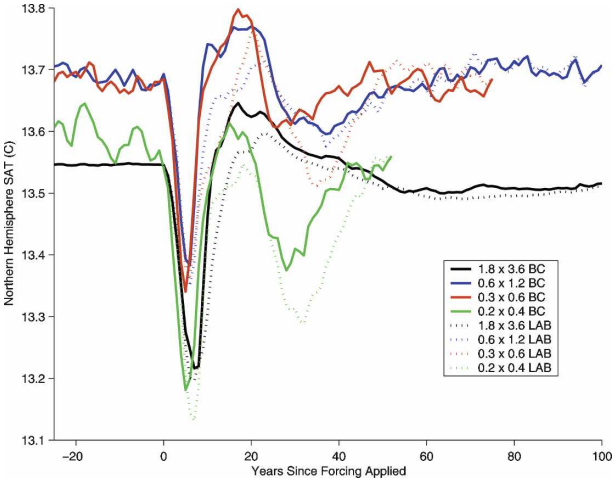

FIG. 9. Northern Hemisphere SAT response to freshwater forcing.

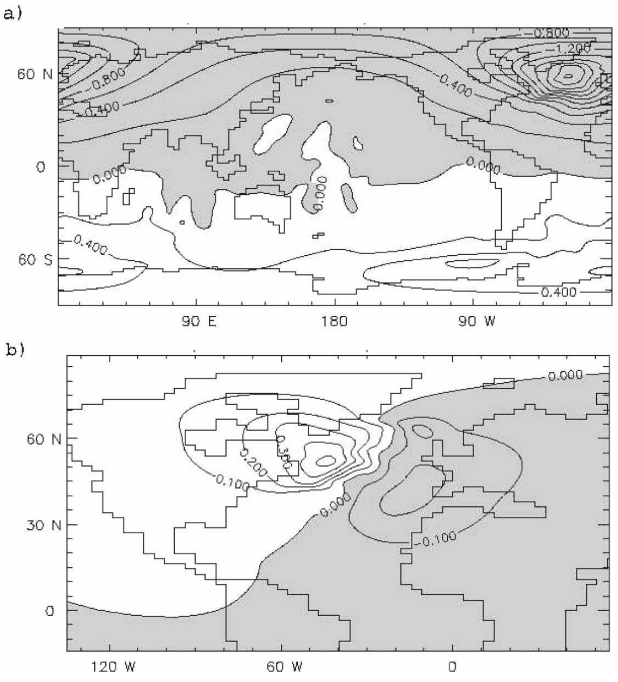

FIG. 10. (a) The global SAT anomalies for the LAB forcing scenario and (b) the BC minus LAB forcing SAT difference in the North Atlantic 5 yr after initial forcing at 0.3° × 0.6° resolution. Shaded regions are negative.

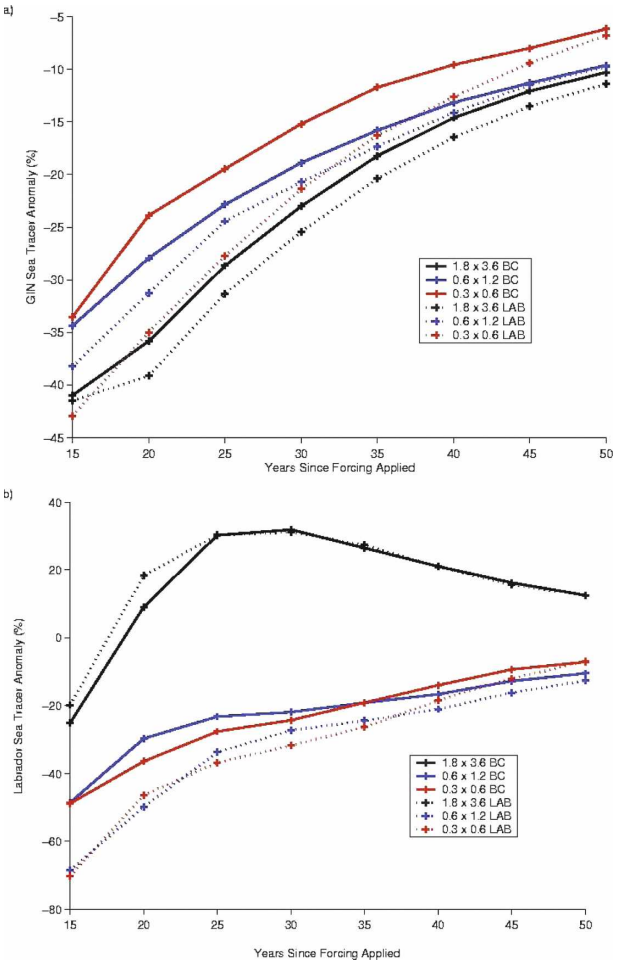

FIG. 11. Percent difference in amount of tracers found below 1000 m in the Atlantic Ocean relative to control runs.

positive difference in the west and negative difference in the east increases from 0.45° to 0.75°C and −0.18° to −0.50°C, respectively, with resolution. A recent study by Saenko et al. (2007) explored the mechanism that led to an extensive area of the subpolar west Atlantic actually warming when freshwater is discharged along the Labrador coast, despite a substantial weakening of the AMOC. They used a coarse-resolution model with ocean and sea ice components similar to ours, but included a more complex atmospheric component that allowed surface wind anomalies to feed back on the ocean. Their experiment also started from a cooler initial state with more extensive Labrador Sea ice coverage, the melting of which is required to amplify the warming response.

c. *NADW tracer anomalies*

The application of tracers in the 1.8 ° × 3.6°, 0.6° × 1.2°, and 0.3° × 0.6° control runs alongside the freshwater forcing runs (refer to section 3d) allows us to separately evaluate the effect of the forcing on NADW formed in both the Labrador and GIN Seas. Tracer anomalies are calculated every 5 yr as the percent difference between the forcing and control runs in the amount of tracers found below 1000 m in the Atlantic. We evaluate anomalies after 15 yr to provide enough time for a significant amount of the tracers to be advected to depth.

The maximum reduction of GIN tracers ranges from 34% to 44% (Fig. 11a). The reduction is smaller in response to BC forcing than to LAB forcing in all three models, with the maximum difference between forcing scenarios increasing from 3% at 1.8° × 3.6° to 11% at 0.3° × 0.6°. In response to the BC forcing, the reduction of GIN tracers is monotonically reduced as horizontal resolution is increased. There is not a consistent dependence on model resolution in the GIN tracer response to LAB forcing.

The reduction of LAB tracers is significantly larger than the reduction of GIN tracers in the 0.6° × 1.2° and 0.3° × 0.6° models (Fig. 11b). With a maximum decrease of 75% in response to LAB forcing and 55% in response to BC forcing for both models, the LAB tracer response is also substantially more dependent on

the forcing scenario in the two higher-resolution models. There is little difference between forcing scenarios in LAB tracer anomalies for the 1.8° × 3.6° model. They increase from −20% to 25% after 25 yr as the result of Labrador Sea convection actually turning on ~10 yr after the initial forcing. It is possible that convective activity in the North Atlantic has multiple stable states, and the forcing may have perturbed the coarse-resolution model from a state where Labrador Sea convection is not favored to one where it is.

It is interesting that the NADW tracer anomalies present a different and perhaps clearer perspective on the influence of horizontal resolution and forcing region than the AMOC strength. Overall, the tracers show a weaker response to BC forcing than to LAB forcing, and this effect is enhanced with increasing resolution. Deep water formation is also more affected in the Labrador Sea than in the GIN Seas. It seems likely that the relative insensitivity of the AMOC response to increasing resolution is partially the result of increased deep convection in close proximity to the freshwater forcing regions in the higher-resolution models.

5. Conclusions

This study investigated the sensitivity of a series of global climate models with increasing horizontal resolution to freshwater forcings similar to the 8.2-kyr event. We began by evaluating the preforcing state of models at 1.8° × 3.6°, 0.6° × 1.2°, 0.3° × 0.6°, and 0.2° × 0.4°. The representation of the barotropic volume transports in the North Atlantic is improved at higher resolution, and the speed of the western boundary currents off the coast of Florida and Labrador is increased by factors of 2 and 5, respectively, from coarsest to highest resolution. Improvements in the meridional heat transport and the poleward penetration of the NAC result in a monotonic reduction in North Atlantic sea ice. While the AMOC remains stable in all models (NADW formation rates in the range of 21–23 Sv), the energy released by Labrador Sea deep convection is increased by roughly an order of magnitude at higher resolution.

The total duration (ranges from 40 to 60 yr) and maximum amplitude (ranges from 4 to 7 Sv) of the AMOC response to freshwater forcing showed little sensitivity to increasing resolution and differing forcing regions. An evaluation of the forcing impact on different regions of NADW formation with tracers highlighted the possibility that increases in Labrador Sea deep convection at higher resolution mitigate the effect of stronger boundary currents and enhanced mixing. There were differences in the pathway of the AMOC response, with boundary current forcing producing significantly higher-amplitude variability in NADW formation than Labrador Sea forcing. A monotonic affect with increasing resolution of less cooling in the subpolar west Atlantic and more cooling in the subpolar east Atlantic was also found in response to the boundary forcing. Because the UVic ESCM employs a simple, vertically integrated atmospheric component, a significant caveat to these results is the possible importance of a more detailed and dynamic representation of the surface winds and storm tracks.

These results are reassuring in showing that the response of a coarse-resolution EMIC to 8.2-kyr event freshwater forcing is comparable to that at ocean eddy-permitting resolutions. While subtle differences exist, the coarse-resolution AMOC response remains robust at finer horizontal resolutions.

Acknowledgments. This research was supported by the NSERC/CFCAS CLIVAR program. Infrastructure support from CFI, NEC, BCKDF, and UVic is also acknowledged. We are grateful to two anonymous reviewers for their insightful comments.

REFERENCES

Alley, R. B., and A. M. Agustsdottir, 2005: The 8k event: Cause and consequences of a major Holocene abrupt climate change. *Quat. Sci. Rev.,* **24,** 1123–1149.

Barber, D. C., and Coauthors, 1999: Forcing of the cold event of 8,200 years ago by catastrophic drainage of Laurentide lakes. *Nature,* **400,** 344–348.

Bauer, E., A. Ganopolski, and M. Montoya, 2004: Simulation of the cold climate event 8200 years ago by meltwater outburst from Lake Agassiz. *Paleoceanography,* **19,** PA3014, doi:10.1029/2004PA001030.

Beckmann, A., C. Böning, C. Koberle, and J. Willebrand, 1994: Effects of increased horizontal resolution in a simulation of the North Atlantic Ocean. *J. Phys. Oceanogr.,* **24,** 326–344.

Bond, G., W. S. Broecker, S. Johnsen, J. McManus, L. Labeyrie, J. Jouzel, and G. Bonani, 1993: Correlations between climate records from North Atlantic sediments and Greenland ice. *Nature,* **365,** 143–147.

——, and Coauthors, 1997: A pervasive millennial-scale cycle in North Atlantic Holocene and glacial climates. *Science,* **278,** 1257–1266.

Böning, C., F. Bryan, W. Holland, and R. Döscher, 1996: Deep-water formation and meridional overturning in a high-resolution model of the North Atlantic. *J. Phys. Oceanogr.,* **26,** 1142–1164.

Broecker, W. S., 1991: The great ocean conveyor. *Oceanography,* **4,** 79–89.

Bryan, F., and R. Smith, 1998: Modelling the North Atlantic circulation: From eddy-resolving to eddy-permitting. *International WOCE Newsletter,* No. 33, WOCE International Project Office, Southampton, United Kingdom, 12–14.

——, C. Böning, and W. Holland, 1995: On the midlatitude circulation in a high-resolution model of the North Atlantic. *J. Phys. Oceanogr.,* **25,** 289–305.

Bryan, K., 1991: Poleward heat transport in the ocean. *Tellus,* **43A,** 104–115.

——, and L. Lewis, 1979: A water mass model of the world ocean. *J. Geophys. Res.,* **84** (C5), 2503–2517.

Canuto, V., A. Howard, P. Hogan, Y. Cheng, M. Dubovikov, and L. Montenegro, 2004: Modeling ocean deep convection. *Ocean Modell.,* **7,** 75–95.

Clarke, G., D. L. J. Teller, and A. Dyke, 2003: Superlakes, megafloods, and abrupt climate change. *Science,* **301,** 922–923.

Dickson, R., and J. Brown, 1994: The production of North Atlantic Deep Water: Sources, rates, and pathways. *J. Geophys. Res.,* **99** (C6), 12 319–12 341.

Duffy, P., M. Wickett, and K. Caldeira, 2002: Effect of horizontal grid resolution on the near-equilibrium solution of a global ocean–sea ice model. *J. Geophys. Res.,* **107,** 3075, doi:10.1029/2000JC000658.

Dukowicz, J. K., and R. Smith, 1994: Implicit free-surface method for the Bryan–Cox–Semtner Ocean Model. *J. Geophys. Res.,* **99** (C4), 7991–8014.

Fanning, A. F., and A. J. Weaver, 1997: A horizontal resolution and parameter sensitivity study of heat transport in an idealized coupled climate model. *J. Climate,* **10,** 2469–2478.

——, and ——, 1998: Thermohaline variability: The effects of horizontal resolution and diffusion. *J. Climate,* **11,** 709–715.

Flatau, M., L. Talley, and P. Niiler, 2003: The North Atlantic Oscillation, surface current velocities, and SST changes in the subpolar North Atlantic. *J. Climate,* **16,** 2355–2369.

Ganachaud, A., and C. Wunsch, 2000: Improved estimates of global ocean circulation, heat transport and mixing from hydrographic data. *Nature,* **408,** 453–457.

——, and ——, 2003: Large-scale ocean heat and freshwater transports during the World Ocean Circulation Experiment. *J. Climate,* **16,** 696–705.

Gent, P., and J. McWilliams, 1990: Isopycnal mixing in ocean circulation models. *J. Phys. Oceanogr.,* **20,** 150–155.

Hibler, W. D., III, 1979: A dynamic thermodynamic sea ice model. *J. Phys. Oceanogr.,* **9,** 815–846.

Hunke, E. C., and J. K. Dukowicz, 1997: An elastic viscous plastic model for sea ice dynamics. *J. Phys. Oceanogr.,* **27,** 1849–1867.

Johns, W., T. Shay, J. Bane, and D. Watts, 1995: Gulf Stream structure, transport, and recirculation near 68°W. *J. Geophys. Res.,* **100** (C1), 817–838.

Kistler, R., and Coauthors, 2001: The NCEP–NCAR 50-Year Reanalysis: Monthly means CD-ROM and documentation. *Bull. Amer. Meteor. Soc.,* **82,** 247–267.

Lavender, K., R. Davis, and W. Brechner Owens, 2002: Observations of open-ocean deep convection in the Labrador Sea from subsurface floats. *J. Phys. Oceanogr.,* **32,** 511–526.

Leverington, D., J. Mann, and J. Teller, 2002: Changes in the bathymetry and volume of glacial Lake Agassiz between 9200 and 7700 ^{14}C yr B.P. *Quat. Res.,* **57,** 244–252.

Lumpkin, R., and K. Speer, 2003: Large-scale vertical and horizontal circulation in the North Atlantic Ocean. *J. Phys. Oceanogr.,* **33,** 1902–1920.

Manabe, S., and R. J. Stouffer, 1995: Simulation of abrupt climate change induced by freshwater input to the North Atlantic Ocean. *Nature,* **378,** 165–167.

Marshall, J., and F. Schott, 1999: Open-ocean convection: Observations, theory and models. *Rev. Geophys.,* **37,** 1–64.

Matthews, H., A. J. Weaver, M. Eby, and K. Meissner, 2003: Radiative forcing of climate by historical land cover change. *Geophys. Res. Lett.,* **30,** 1055, doi:10.1029/2002GL016098.

McAvaney, B., and Coauthors, 2001: Model evaluation. *Climate Change 2001: The Scientific Basis,* J. T. Houghton et al., Eds., Cambridge University Press, 471–524.

Meissner, K., and P. Clark, 2006: Impact of floods versus routing events on the thermohaline circulation. *Geophys. Res. Lett.,* **33,** L15704, doi:10.1029/2006GL026705.

Morrill, C., and M. Jacobsen, 2005: How widespread were climate anomalies 8200 years ago? *Geophys. Res. Lett.,* **32,** L19701, doi:10.1029/2005GL023536.

Oschlies, A., 2002: Improved representation of upper-ocean dynamics and mixed layer depths in a model of the North Atlantic on switching from eddy-permitting to eddy-resolving grid resolution. *J. Phys. Oceanogr.,* **32,** 2277–2298.

Pacanowski, R., 1995: MOM 2 documentation: User's guide and reference manual. GFDL Ocean Group Tech. Rep. 3, 232 pp.

Rahmstorf, S., 2002: Ocean circulation and climate during the past 120,000 years. *Nature,* **419,** 207–214.

Renssen, H., H. Goosse, T. Fichefet, and J.-M. Campin, 2001: The 8.2 kyr BP event simulated by a global atmosphere–sea-ice–ocean model. *Geophys. Res. Lett.,* **28,** 1567–1570.

——, ——, and ——, 2002: Modeling the effect of freshwater pulses on the early Holocene climate: The influence of high-frequency climate variability. *Paleoceanography,* **17,** 1020, doi:10.1029/2001PA000649.

Saenko, O., A. J. Weaver, D. Robitaille, and G. Flato, 2007: Warming of the subpolar Atlantic triggered by freshwater discharge at the continental boundary. *Geophys. Res. Lett.,* **34,** L15604, doi:10.1029/2007GL030674.

Smethie, W., and R. Fine, 2001: Rates of North Atlantic Deep Water formation calculated from chlorofluorocarbon inventories. *Deep-Sea Res. I,* **48,** 189–215.

Smith, R., M. Maltrud, F. Bryan, and M. Hecht, 2000: Numerical simulation of the North Atlantic at 1/10°. *J. Phys. Oceanogr.,* **30,** 1532–1561.

Stammer, D., 1997: Global characteristics of ocean variability from regional TOPEX/Poseidon altimeter measurements. *J. Phys. Oceanogr.,* **27,** 1743–1769.

Stocker, T., 1998: Climate change: The seesaw effect. *Science,* **282,** 61–62.

Stommel, H., 1961: Thermohaline convection with two stable regimes of flow. *Tellus,* **13,** 224–230.

Stouffer, R., and Coauthors, 2006: Investigating the causes of the response of the thermohaline circulation to past and future climate changes. *J. Climate,* **19,** 1365–1387.

Talley, L., 2003: Shallow, intermediate, and deep overturning components of the global heat budget. *J. Phys. Oceanogr.,* **33,** 530–560.

——, J. Reid, and P. Robbins, 2003: Data-based meridional overturning streamfunctions for the global ocean. *J. Climate,* **16,** 3213–3226.

Treguier, A., S. Theetten, E. Chassignet, T. Penduff, R. Smith, L. Talley, J. Beismann, and C. Böning, 2005: The North Atlantic subpolar gyre in four high-resolution models. *J. Phys. Oceanogr.,* **35,** 757–774.

Von Grafenstein, U., H. Erlenkeuser, J. Müller, J. Jouzel, and S.

Johnsen, 1998: The cold event 8200 years ago documented in oxygen isotope records of precipitation in Europe and Greenland. *Climate Dyn.,* **14,** 73–81.

Wang, Y., and L. Mysak, 2005: Response of the ocean, climate and terrestrial carbon cycle to Holocene freshwater discharge after 8 kyr BP. *Geophys. Res. Lett.,* **32,** L15705, doi:10.1029/2005GL023344.

Weaver, A. J., and T. M. Hughes, 1992: Stability and variability of the thermohaline circulation and its link to climate. *Trends Phys. Oceanogr.,* **1,** 15–70.

——, and Coauthors, 2001: The UVic Earth System Climate Model: Model description, climatology, and applications to past, present and future climates. *Atmos.–Ocean,* **39,** 361–428.

Willebrand, J., and Coauthors, 2001: Circulation characteristics in three eddy-permitting models of the North Atlantic. *Prog. Oceanogr.,* **48,** 123–161.

Wunsch, C., 1999: Where do ocean eddy fluxes matter? *J. Geophys. Res.,* **104C,** 13 235–13 249.

——, 2007: The past and future ocean circulation from a contemporary perspective. *Ocean Circulation: Mechanisms and Impacts; Past and Future Changes of Meridional Overturning, Geophys. Monogr.,* Vol. 173, Amer. Geophys. Union, 53–74.